Article ID: 1007-7294(2024)12-1835-14

# Marine Predator Algorithm-based Sliding Mode Control of a Novel Motion Simulator for High Column Sloshing Experiments

*DU Zun-feng*[1], *CHEN Xiang-yu*[2], *BAI Hao*[3], *ZHU Hai-ming*[1], *HAN Mu-xuan*[1]

(1. State Key Laboratory of Hydraulic Engineering Intelligent Construction and Operation, School of Civil Engineering, Tianjin University, Tianjin 300350, China; 2. Power China Northwest Engineering Corporation Limited, Xi'an 710065, China; 3. Nanhai Engineering Branch, CNOOC Energy Development Equipment Technology Co., Ltd., Zhanjiang 524057, China)

**Abstract:** Sloshing experiment is crucial to determine the reaction performance of regeneration columns on an offshore floating platform. A novel type of column motion simulating device and a Marine Predator Algorithm-based Sliding Mode Controller (MPA-SMC) are proposed for such sloshing experiments. The simulator consists of a Stewart platform and a steel framework. The Stewart platform is located at the column's center of gravity (CoG) and supported by the steel framework. The platform's hydraulic servo system is controlled by a sliding mode controller with parameters optimized by MPA to improve robustness and precision. A numerical sloshing experiment is conducted using the proposed device and controller. The results show that the novel motion simulator has lower torque during the column sloshes, and the proposed controller performs better than a well-tuned PID controller in terms of target tracking precision and anti-interference capability.

**Key words: regeneration column; sloshing experiment; motion simulator; Stewart platform; sliding mode control; marine predator algorithm**

**CLC number:** TE952 **Document code:** A **doi:** 10.3969/j.issn.1007-7294.2024.12.003

## 0 Introduction

Over the last few decades, floating platforms such as the FLNG (Floating Liquefied Natural Gas) system and the FPSO (Floating Production, Storage, and Offloading) unit have been developed and used to extract deep-water natural gas resources. However, traditional deacidification pretreatment equipment is designed for land applications, with less consideration given to the offshore operating condition on floating platforms. In harsh marine environments, the motion of the floating plat-

Received date: 2024-06-22

Foundation items: Supported by National Key Research and Development Program of China (2022YFC2806300); the National Natural Science Foundation of China (51109158); Transportation Science and Technology Development Project of Tianjin (2022-48); Tianjin University Graduate Education Special Found 2021 Projects (C1-2021-004); Tianjin Research Innovation Project for Postgraduate Students (2022BKY077)

Biography: DU Zun-feng(1984-), male, ph.D., associate professor; CHEN Xiang-yu(1997-), female, master, assistant engineer; BAI Hao(1986-), male, senior engineer; ZHU Hai-ming(1992-), male, Ph.D., assistant research fellow; HAN Mu-xuan(1996-), female, Ph.D. candidate, corresponding author, E-mail: hanmuxuan@tju.edu.cn.

forms is transmitted to the onboard equipment. Columns, being most susceptible to this motion, are crucial for maintaining stability[1]. The effectiveness of column reactions highly depends on the contact quality between the descending liquid and the rising vapor, as inclination can lead to undesired liquid maldistribution inside columns[2]. The gas deacidification plate column and its typical placement on a floating platform are illustrated in Fig.1.

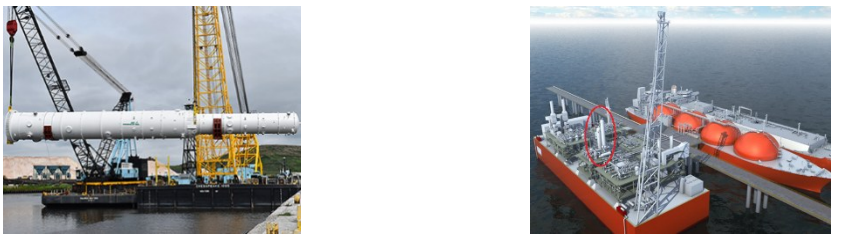

(a) Column (b) Floating platform

Fig.1 Plate column and its typical placement on a floating platform

There have been numerous studies focusing on column performance under ship motions. Some numerical simulations have been conducted to investigate liquid maldistribution in columns using computational fluid dynamics models[3-4]. Building upon this foundation, experimental methods have been widely employed. Hanawa et al[5] experimented with a single-axis rotating apparatus and a packed amine column with a height of 4 m to reveal how FPSO motions influence the reaction performance of the column. Son et al[2] measured the CO2 absorption performance of a column with a diameter of 0.4 m and a packed height of 4 m installed on an FLNG. They found that roll motion can affect the absorption performance of the column under certain conditions. Similar experiments conducted were reported in Ref.[6], of which the authors investigated the effects of tilt, roll, heave and sway motions on the mass transfer area of a pilot-scale column with a diameter of 0.8 m and a height of 1.5 m. As a common practice, the platform is installed at the column bottom and sloshes the column as it moves.

However, an issue arises with this traditional column experimental layout. A column is generally designed with a significant height and a thin shape to ensure complete reactions. Consequently, the center of gravity (CoG) of the column is elevated, which may cause a deviation in the CoG when the platform is only slightly rotated. In Fig.2, the offset refers to the horizontal distance from the center of the Stewart top platform to the CoG of the column. Due to the column's weight, even a slight offset can exert considerable torque on the Stewart platform. If the torque acted on the Stewart platform is inadequate, the column may tilt and collapse, posing a safety risk for tall columns. Therefore, no matter whether it is a model test column or a realistic column, its height is often limited for safety reasons.

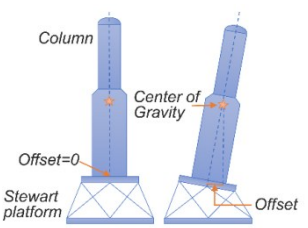


Fig.2 Traditional motion simulator for column sloshing experiments

Another challenging problem concerns the control of motion simulators for tall columns. These simulators typically utilize hydraulic system to achieve high rigidity and substantial load capacity[7]. The hydraulic system, a complex large-scale network comprising numerous components and pipe-

lines, introduces nonlinear elements that can affect the stability and accuracy of the control system[8]. These complexities necessitate a robust and stable control mechanism for motion simulators. While a PID controller is often sufficient for experimental purposes, it fails to account for nonlinear characteristics and is ineffective against disturbances[9]. Among modern control methods, the Sliding Mode Control (SMC) strategy has a better performance in stability and robustness due to its independence on the mathematical model[10]. Guo et al[11] proposed the SMC method for a hydraulically driven 6-DOF Stewart platform, demonstrating satisfactory position-tracking behavior. Cai et al[12] extended this to a velocity feedforward SMC controller for a ship-deck-mounted Stewart platform, effectively rejecting motion disturbances in simulation.

However, specifying the SMC parameters in SMC design is challenging because they are chosen based on a wealth of experience. A novel meta-heuristic optimization Marine Predator Algorithm (MPA)[13] was first proposed in 2020. The main idea of MPA is that marine predators achieve an optimal hunting state through foraging strategies of Lévy flight and Brownian motion, providing an efficient optimization framework. Recently, MPA has been effectively employed in power system controlling[14] and other engineering fields, as it demonstrates a faster convergence speed and a greater accuracy than Ant Colony Optimization, Particle Swarm Optimization and other algorithms[13]. However, it is still not used to solve complex motion-simulating control problems.

To this end, the present paper proposes a novel motion simulator for sloshing experiments of higher columns and the MPA-optimized SMC method (MPA-SMC) for the proposed simulator. The remainder of this paper is arranged as follows. Chapter 1 focuses on the description of the novel motion simulator, followed by the description of the simulator modeling in Chapter 2 and the MPA-SMC method of the simulator in Chapter 3, while the results and discussions are provided in Chapter 4. The conclusions are drawn in Chapter 5.

## 1 Description of the novel motion simulator

Fig.3 illustrates the proposed novel motion simulator, which consists of a Stewart platform and a steel framework. The Stewart platform includes a top platform, a bottom platform, six extensible legs and motion joints to connect platforms and legs. Generally, the top platform is movable while the bottom platform is fixed for simulation purposes. In this motion simulator, the Stewart top platform is installed at the CoG level of the column to reduce offset when the column sloshes. To firmly unite the Stewart top platform and the column, six skirts are welded on the column and connected with the top platform through enhanced bolts, the sizes of which can be determined according to industrial standards.

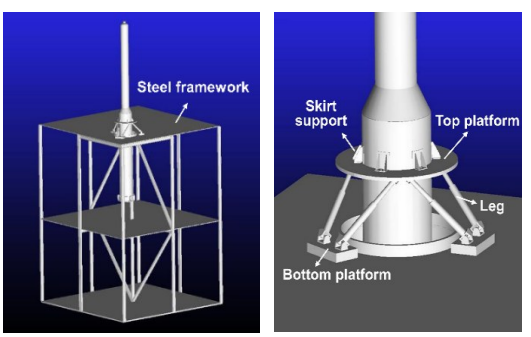


Fig.3 Novel motion simulator

The steel framework serves as the base for both the Stewart platform and the column, and can be reused in a production facility after the column sloshing experiment is completed. The Stewart platform is installed on the top deck of this steel framework, requiring reinforcement plates and stiffeners. Moreover, the top deck is designed to allow a circular opening for the column to pass through and slosh. The remaining space on the top deck and the middle deck of the steel framework is reserved for other supporting equipment including boilers, tanks, line pipes, pumps and measuring instruments. The structural dimension of the motion simulator is usually determined by the size and the weight of the column. In this paper, a regeneration column is used for sloshing experiments, the detailed information of which is shown in Tab.1. The full water weight in the table is assumed to be the load capacity of the motion simulator.

**Tab.1 Parameters for the regeneration column**

| Regeneration column parameter /unit | Value |
|---|---|
| Height /m | 16.64 |
| Upper part diameter /m | 0.6 |
| Lower part diameter /m | 1.0 |
| Net weight /kg | 5003 |
| Full water weight /kg | 15000 |
| Packed volume /$m^3$ | 1.73 |
| Column′s CoG level /m | 7.0 |

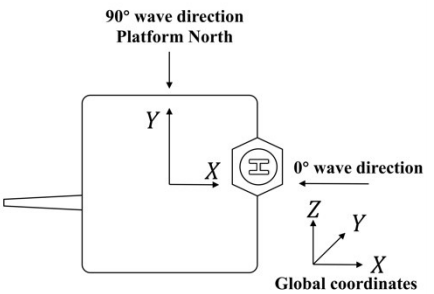


Fig.4 Coordinate of the semi-submersible platform

The desired motion of the simulator involves the regeneration column's motion on floating platforms, which can be simplified to the motion of a deep-draft semi-submersible platform where the column will be mounted. Fig.4 shows the coordinate of the semi-submersible platform. The origin of the platform's coordinate is at the water surface, with the $Z$-axis pointing straight upward.

The column will suspend operation under extreme sea conditions, therefore, as the most hazardous state, the fourth sea state is chosen as the column sloshing condition. Tab.2 shows the simulator′s motion requirements determined on the basis of motion response data of the floating platform under the fourth sea state. In terms of the simulator′s parameters, the diameters of the Stewart top platform and bottom platforms are 2.6 m and 4.6 m respectively. The length of the hydraulic actuating cylinder is 1.65 m according to the standard GB2348-2018, with a piston rod length of 1.5 m. Additionally, the height and the side length of the steel framework unit are 7 m and 5 m respectively.

**Tab.2 Specifications for the simulator**

| | Displacement range | Period scope |
|---|---|---|
| Surge, Sway, Heave | ± 0.25 m | ≥8 s |
| Roll, Pitch, Yaw | ± 2.5° | ≥8 s |

## 2 Mathematical modeling of the motion simulator

### 2.1 Kinematics analysis

A local reference frame $O_s(x, y, z)$ attached to the top platform and a fixed frame $O_f(x, y, z)$ at-

tached to the bottom are defined, as shown in Fig.5.

Input variables are selected as $\boldsymbol{q} = [x, y, z, \alpha, \beta, \gamma]$, which represent the position and orientation of the top platform. The $i$th leg vector $\boldsymbol{L}_i$ with respect to the fixed frame can be denoted as

$$\boldsymbol{L}_i = \boldsymbol{R}_i\boldsymbol{S}_i + \boldsymbol{T}_i - \boldsymbol{F}_i \tag{1}$$

where, $\boldsymbol{S}_i$ denotes the position vector of the $i$th upper joint in reference frame, $\boldsymbol{F}_i$ denotes the position vector of the $i$th base joint, and $\boldsymbol{R}_i$ represents the rotation matrix defined as follows:

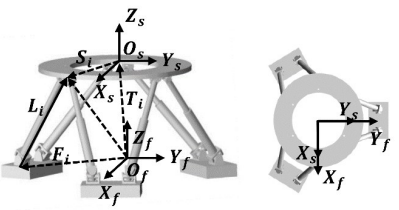


Fig.5 Coordinate system of the Stewart platform

$$\boldsymbol{R}_i = \begin{bmatrix} 1 & 0 & 0 \\ 0 & \cos\alpha & -\sin\alpha \\ 0 & \sin\alpha & \cos\alpha \end{bmatrix} \begin{bmatrix} \cos\beta & 0 & -\sin\beta \\ 0 & 1 & 0 \\ \sin\beta & 0 & \cos\beta \end{bmatrix} \begin{bmatrix} \sin\gamma & \cos\gamma & 0 \\ \cos\gamma & -\sin\gamma & 0 \\ 0 & 0 & 1 \end{bmatrix} \tag{2}$$

Besides, $\boldsymbol{T}_i$ denotes the translation vector of the origin of the top platform with respect to the fixed frame, and it is denoted as

$$\boldsymbol{T}_i = \begin{bmatrix} x & 0 & 0 \\ 0 & y & 0 \\ 0 & 0 & z \end{bmatrix} \tag{3}$$

Then, the length of the $i$th leg can be computed by the Euclidean norm as follows:

$$l_i = \left\| \boldsymbol{L}_i \right\| \tag{4}$$

### 2.2 Modeling of hydraulic actuator

Fig.6 shows the scheme of a hydraulic servo system, which consists of an asymmetric hydraulic cylinder and a three-position four-way servo valve. The area ratio of the piston is $n = A_2/A_1$, where $A_1$ and $A_2$ are effective working areas at the non-piston and piston sides. $P_1$ and $P_2$ are the forward and return pressures in the cylinder. Thereby, the load pressure $P_{\mathrm{L}} = (A_1P_1 - A_2P_2)/A_1 = P_1 - nP_2$, and the load flow $Q_{\mathrm{L}} = Q_1$ according to the cylinder′s out power $N = P_1Q_1 - P_2Q_2 = (P_1 - nP_2)Q_1 = P_{\mathrm{L}}Q_{\mathrm{L}}$.

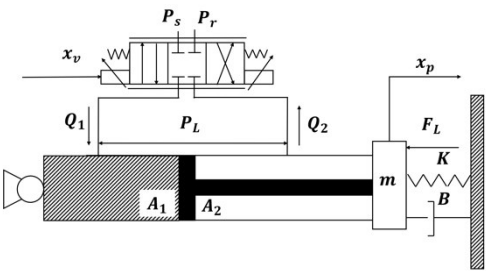


Fig.6 Scheme of hydraulic servo system

The dynamic model of the hydraulic servo system is made up of three parts[15]. The force balance equation on the actuating piston of the cylinder is given as follows:

$$A_1P_{\mathrm{L}} = m\ddot{x}_{\mathrm{p}} + B\dot{x}_{\mathrm{p}} + Kx_{\mathrm{p}} + F_{\mathrm{L}} \tag{5}$$

where, $x_{\mathrm{p}}$ means the piston displacement, $m$ represents the total mass of the piston and the load referred to the piston, $B$ denotes the viscous damping coefficient of the piston and the load, $K$ denotes the load spring gradient, $P_{\mathrm{L}}$ denotes the load pressure, and $F_{\mathrm{L}}$ denotes the load force acting on the piston.

With hypotheses that the pressure in each chamber is the same anywhere as well as the temperature and density are constant, the cylinder flow continuity equation can be given as follows:

$$Q_{\mathrm{L}} = A_1 \dot{x}_p + C_{tp} P_{\mathrm{L}} + \frac{V_t}{4\beta_t} \dot{P}_{\mathrm{L}} \tag{6}$$

where, $Q_{\mathrm{L}}$ refers to the load flow, $V_t$ is the initial volume of the chamber, $\beta_t$ is the effective bulk modulus of the system, and $C_{tp}$ is a leakage coefficient of the piston.

For the spool valve, its linearized flow equation can be written as

$$Q_{\mathrm{L}} = K_q x_v - K_c P_{\mathrm{L}} \tag{7}$$

where $x_v$ is assumed as the spool valve core displacement, $K_c$ is the flow-pressure coefficient, and $K_q$ is the flow gain coefficient of the valve.

Eqs.(5)-(7) completely describe a third order dynamics of the hydraulic servo system of the Stewart platform. By combining these three equations and defining $\boldsymbol{X} = [x_1, x_2, x_3]' = [x_p, \dot{x}_p, \ddot{x}_p]'$, the corresponding state space function of the hydraulic actuators can be written as follows:

$$\begin{cases} \dot{x}_1 = x_2 \\ \dot{x}_2 = x_3 \\ \dot{x}_3 = a_1 x_1 + a_2 x_2 + a_3 x_3 + bu + d \end{cases} \tag{8}$$

where, $a_1 = -\dfrac{4\beta_t K_{ce} K}{V_t m}$, $a_2 = -\left(\dfrac{4\beta_t K_{ce} B}{V_t m} + \dfrac{4\beta_t A_1^2}{V_t m} + \dfrac{K}{m}\right)$, $a_3 = -\left(\dfrac{4\beta_t K_{ce}}{V_t} + \dfrac{B}{m}\right)$, $b = -\dfrac{4\beta_t K_q A_1}{V_t m}$, $d = -\left(\dfrac{4\beta_t K_{ce}}{V_t m} F_L + \dfrac{1}{m} \dot{F}_L\right)$, $K_{ce} = K_c + K_{tp}$.

## 3 Control of the motion simulator

Based on the dynamic model of the hydraulic actuators, the MPA-SMC method is proposed for Stewart leg actuator control.

### 3.1 Sliding mode controller design

Given $x_d$ as the target position signal, an error between the desired position and the state variables of the actuating leg is defined as

$$\begin{cases} e_1 = x_d - x_1 \\ e_2 = \dot{x}_d - x_2 \\ e_3 = \ddot{x}_d - x_3 \end{cases} \tag{9}$$

The sliding surface can be described as follows:

$$s = \left(\frac{\mathrm{d}}{\mathrm{d}t} + \lambda\right)^{n-1} e_1 \tag{10}$$

where $\lambda$ is a positive constant and can transform the $n$th-order tracking problem into an equivalent 1st-order stabilization problem[16]. For $n = 3$, Eq.(10) is rearranged as

$$s = \lambda^2 e_1 + 2\lambda e_2 + e_3 \tag{11}$$

Then, the derivative of $s$ is obtained as follows:

$$\dot{s} = \lambda^2 e_2 + 2\lambda e_3 + \dddot{x}_d - \dddot{x}_1 \tag{12}$$

Substituting Eq.(8) to Eq.(12) yields

$$\dot{s} = \lambda^2 e_2 + 2\lambda e_3 + \dddot{x}_d - a_1 x_1 - a_2 x_2 - a_3 x_3 - bu - d \tag{13}$$

To improve the reaching performance of the sliding surface and eliminate chattering from the control voltage, an exponential reaching law[17] is designed as

$$\dot{s} = -\eta \operatorname{sgn}(s) - ks \tag{14}$$

where, $\eta > 0$ and $k > 0$.

Therefore, the best approximation of a continuous control voltage $u$ can be obtained by achieving $\dot{s} = 0$.

$$u = \frac{1}{b}\left(\lambda^2 \dot{e} + 2\lambda \ddot{e} + \dddot{x}_d - a_1 x_1 - a_2 x_2 - a_3 x_3 - d + \eta \operatorname{sgn}(s) + ks\right) \tag{15}$$

To prove the stability of the control system, the Lyapunov function is defined as

$$V = \frac{1}{2} s^2 \tag{16}$$

The derivation of Eq.(16) is

$$\dot{V} = s\dot{s} = s\left(-\eta \operatorname{sgn}(s) - ks\right) \leqslant -ks^2 \tag{17}$$

Finally, the following convergence effect is derived with the lemma[18].

$$V_{(t)} \leqslant e^{-k\left(t - t_{(0)}\right)} V_{t_{(0)}} \tag{18}$$

As can be observed, both $V_{(t)}$ and $s$ are convergent, indicating that the control system is stable.

### 3.2 Marine predator algorithm for parameter optimization

Parameters of $\lambda$, $\eta$ and $k$ in the processing of the SMC design are obtained through an optimization method called Marine Predator Algorithm (MPA). Fig.7 depicts the flowchart of MPA.

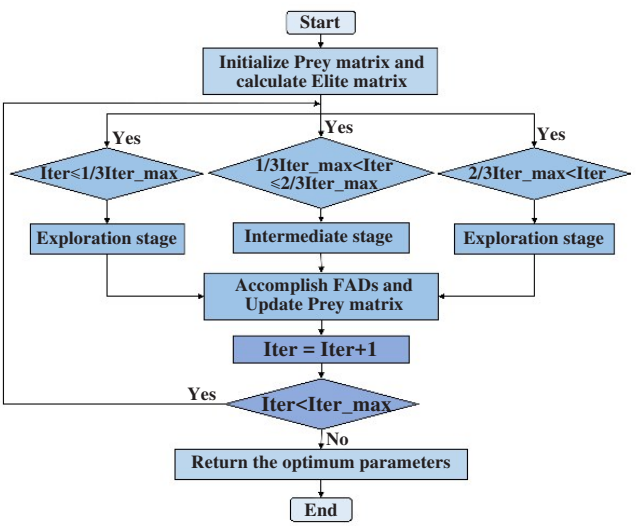


Fig.7 Flowchart of MPA[19]

In MPA, the initial population $X_0$ is generated in the search space.

$$X_0 = X_{\min} + rand\left(X_{\max} - X_{\min}\right) \tag{19}$$

where, $X_{\max}$ and $X_{\min}$ are the upper and lower limits of each variable, and *rand* means a uniform random vector between 0 and 1.

A Prey matrix ($M_{\text{Prey}}$) is built firstly to contain all individuals, and the individuals with the best fitness value from the prey matrix are recorded as a top predator vector, which is described as an Elite matrix ($M_{\text{Elite}}$).

$$\boldsymbol{M}_{\text{Prey}}=\begin{bmatrix}X_{1,1} & \cdots & X_{1,d}\\ \vdots & \cdots & \vdots\\ X_{n,1} & \cdots & X_{n,d}\end{bmatrix}, M_{\text{Elite}}=\begin{bmatrix}X_{1,1} & \cdots & X_{1,d}\\ \vdots & \cdots & \vdots\\ X_{n,1} & \cdots & X_{n,d}\end{bmatrix} \tag{20}$$

The fitness value increases as the error function decreases. In particular, the error function is assumed to be the Integral of the Absolute Error value (IAE), and the control amount is also included in the error function, as shown in Eq.(21).

$$E=\int_0^T\left(0.99t\left|e(t)\right|+0.01u^2(t)\right)\mathrm{d}x \tag{21}$$

According to the different velocity ratios between the predator and the prey, three iterative phases are divided. In the exploration phase, the prey moves faster than the predator. The latter's motion is assumed to maintain the status quo as a Brownian walk. The position of prey is, when $Iter \leqslant \frac{1}{3} Iter\_\max$, updated by

$$\begin{cases}\overrightarrow{r_{\text{stepsize}_i}}=\overrightarrow{R_B}\otimes\left(\overrightarrow{X_{\text{Elite}_i}}-\overrightarrow{R_B}\times\overrightarrow{X_{\text{Prey}_i}}\right), i=1,2,3,\ldots,n\\ \overrightarrow{X_{\text{Prey}_i}}=\overrightarrow{X_{\text{Prey}_i}}+P.\overrightarrow{R_L}\otimes\overrightarrow{r_{\text{stepsize}_i}}, P=0.5\end{cases} \tag{22}$$

where, $R\in[0,1]$ means a random vector, and $\overrightarrow{R_B}$ represents the Brownian motion vector.

The second is an intermediate phases, $\frac{1}{3} Iter\_\max \leqslant Iter \leqslant \frac{2}{3} Iter\_\max$, in which both predator and the prey move at the same speed. The predator is following a Brownian motion for global exploration, while the prey changes its motion pattern to Lévy flight for local development. Thus, the whole population is partitioned into two halves.

$$\begin{cases}\overrightarrow{r_{\text{stepsize}_i}}=\overrightarrow{R_L}\otimes\left(\overrightarrow{X_{\text{Elite}_i}}-\overrightarrow{R_L}\times\overrightarrow{X_{\text{Prey}_i}}\right), i=1,\ldots,\frac{n}{2}\\ \overrightarrow{X_{\text{Prey}_i}}=\overrightarrow{X_{\text{Prey}_i}}+P.\overrightarrow{R_L}\otimes\overrightarrow{r_{\text{stepsize}_i}}, P=0.5\end{cases} \tag{23}$$

where $R_L$ is a random vector based on Lévy distribution.

$$\begin{cases}\overrightarrow{r_{\text{stepsize}_i}}=\overrightarrow{R_B}\otimes(\overrightarrow{R_B}\otimes(\overrightarrow{X_{\text{Elite}_i}}-\overrightarrow{X_{\text{Prey}_i}}), i=\frac{n}{2},\ldots,n\\ \overrightarrow{X_{\text{Prey}_i}}=\overrightarrow{Elite_i}+P.CF\otimes\overrightarrow{r_{\text{stepsize}_i}}, CF=\left(1-\frac{Iter}{Iter\_\max}\right)^{\frac{2Iter}{Iter\_\max}}\end{cases} \tag{24}$$

The third phase occurs when $Iter > \frac{2}{3} Iter\_\max$, in which the predators select Lévy flight for a partial exploitation and move faster than the prey. The prey's position is represented by

$$\begin{cases}\overrightarrow{r_{\text{stepsize}_i}}=\overrightarrow{R_L}\otimes(\overrightarrow{R_L}\otimes(\overrightarrow{X_{\text{Elite}_i}}-\overrightarrow{X_{\text{Prey}_i}}), i=1,2,\ldots,n\\ \overrightarrow{X_{\text{Prey}_i}}=\overrightarrow{X_{\text{Elite}_i}}+P.CF\otimes\overrightarrow{r_{\text{stepsize}_i}}\end{cases} \tag{25}$$

The predator's behavior can change to the effect of eddy formation and Fish Aggregating Devices (FADs), which is presented as

$$\overrightarrow{X_{\text{Prey}_i}}=\begin{cases}\overrightarrow{X_{\text{Prey}_i}}+CF\left[\overrightarrow{X_{\min}}+\vec{R}\otimes\left(\overrightarrow{X_{\max}}-\overrightarrow{X_{\min}}\right)\right]\otimes\vec{U}, & \text{if } r\leqslant FADs\\ \overrightarrow{X_{\text{Prey}_i}}+\left[FADs(1-r)+r\right]\left(\overrightarrow{X_{\text{Prey}_{r1}}}-\overrightarrow{X_{\text{Prey}_{r2}}}\right), & \text{if } r>FADs\end{cases} \tag{26}$$

where, FADs reaches an optimization target when $FADs = 0.2$ is the probability. $\vec{U}$ is a random binary solution in $[0,1]$, $r \in [0,1]$ means the uniform random number, $\overrightarrow{X_{\max}}$ and $\overrightarrow{X_{\min}}$ are upper and lower limits of a vector dimension, and $r1$ and $r2$ are random exponents of the prey matrix.

## 4 Simulation and results

### 4.1 Motion simulation for sloshing experiments

The sloshing experiments simulate the motion of the column in irregular waves. One of the semi-submersible platforms operating in sea states with high occurrence frequency and typicality is selected for simulation analysis, in which the wave moves from the northeast with a significant wave height of 1.51 m and a peak frequency of 8.5 Hz, and the surface current speed and the wind speed are 0.39 m/s and 6.86 m/s, respectively. The column′s motion under this operating sea condition, as shown in Fig.8(a), is taken as the desired driving motion for the simulator, within its operational motion range. Sway and surge motions are excluded due to their minimal impact on the column′s reaction performance. Therefore, these two DOFs are limited to zero due to their unnecessary effect on working degrees[4]. In the paper, a dynamic model is built in Adams software to calculate the leg positions of the Stewart platform, as shown in Fig.8(b).

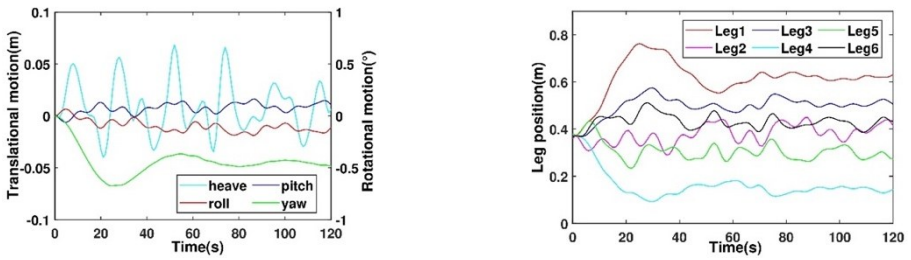


(a) Column′s motion to be simulated (b) Leg positions of the motion simulator

Fig.8 Motions of the Stewart top platform and its legs

Additionally, the torque for the Stewart platform legs of the novel motion simulator is obtained. The torque is compared with the torque result of a traditional motion simulator, as described in Fig.2. Given that the motion of both simulators is the same, the torque on the proposed motion simulator is reduced to a lesser extent, as illustrated in Fig.9. It is proved that the new motion simulator is much safer than a traditional simulator for tall column sloshing.

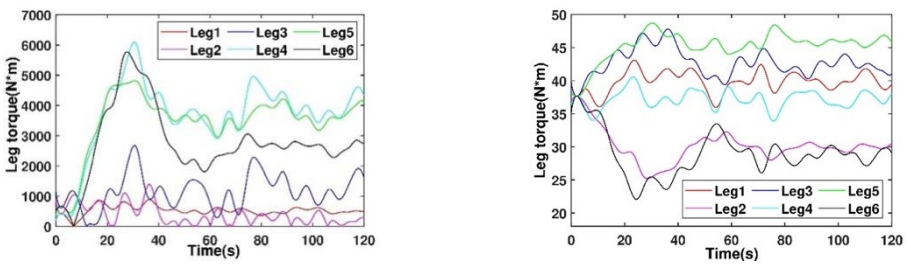


(a) Novel motion simulator (b) Traditional motion simulator

Fig.9 Leg torques on the traditional and novel motion simulators

### 4.2 Controller performances

Numerical simulations are implemented using MATLAB/Simulink to verify the effectiveness of

the MPA-SMC method before the experimental apparatus is applied. Parameters for the hydraulic actuators of the motion simulator are shown in Tab.3. In MPA, *Iter*_max and population size are set to 30 and 50, respectively. At the same time, the lower and upper bounds of $\lambda$, $\eta$, and $k$ in SMC design are [0, 200], [0, 50], and [0, 10] through abundant tests. Fig.10 describes the iterative curves of the above three parameters optimized by MPA and the error function curve. The ability of MPA to seek optimization within the target range is vital. After the twentieth iteration, it basically reaches stability. The final optimal result is [149, 34, 3.5], and the error function value is 42.083. As a comparison, an optimized PID controller is also constructed in MATLAB/Simulink, whose proportional, integral and derivative values have been self-tuned at [11.8, 61.9, −0.04] using the PID self-tuning tool.

**Tab.3 Specifications for the simulator**

| Parameter | Value | Parameter | Value |
|---|---|---|---|
| $\beta_t$ | $6.9\times10^8$ N/m$^2$ | $m$ | 2567.43 kg |
| $K_c$ | $1.78\times10^{-11}$ m$^5$/N·s | $B$ | $1\times10^5$ N·s/ m |
| $C_{tp}$ | $1.2\times10^{-12}$ m$^5$/N·s | $A_P$ | 0.03801 m$^2$ |
| $K$ | 0 N/m | $p_S$ | $2.5\times10^7$ N/m$^2$ |
| $V_t$ | 0.0266 m$^3$ | $K_q$ | 0.2083 m$^3$/A·s |

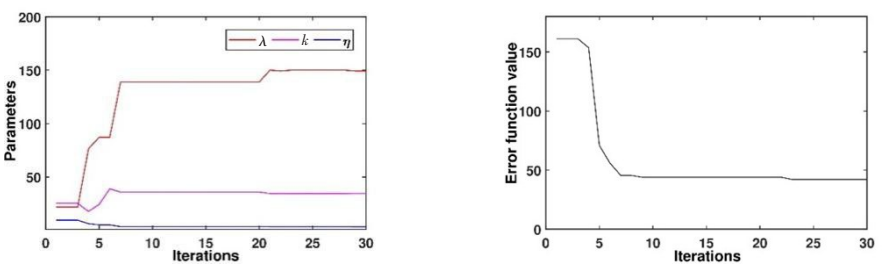


(a) Optimized parameters (b) Fitness function value

Fig.10 Optimization result by MPA

4.2.1 Position tracking capability

Fig.11 exhibits the position tracking outcomes of the legs on the motion simulator by two different controllers, where the red curve refers to the tracking trajectory of MPA-SMC, and the blue curve indicates the tracking trajectory of the PID controller. Two curves overlap with the black one, representing the desired position signal of the Stewart platform legs, indicating that both controllers can track the legs′ positions effectively. Additionally, the tracking error of six legs is displayed in Fig.12. Both MPA-SMC and PID controllers can achieve an extremely high tracking accuracy within $1\times10^{-4}$ m.

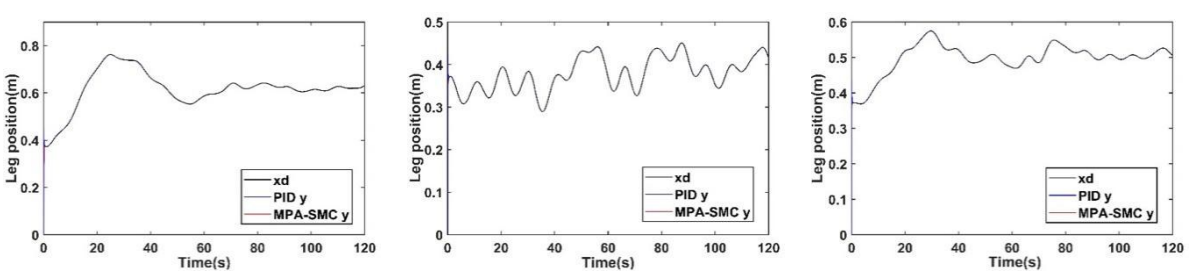


(a) Leg 1 position (b) Leg 2 position (c) Leg 3 position

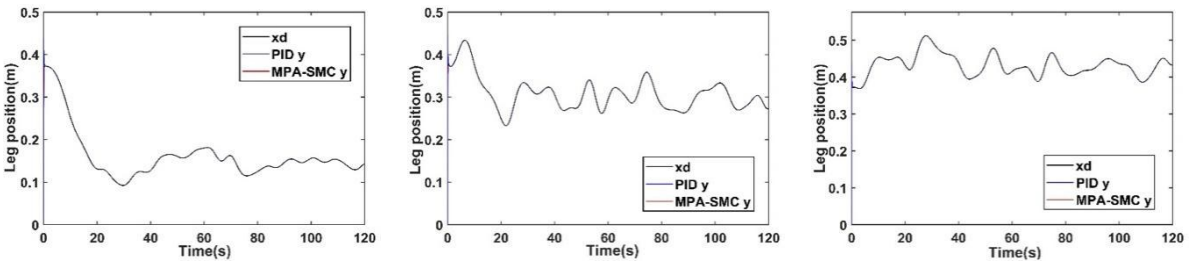


(d) Leg 4 position (e) Leg 5 position (f) Leg 6 position

Fig.11 Position tracking results of two control methods

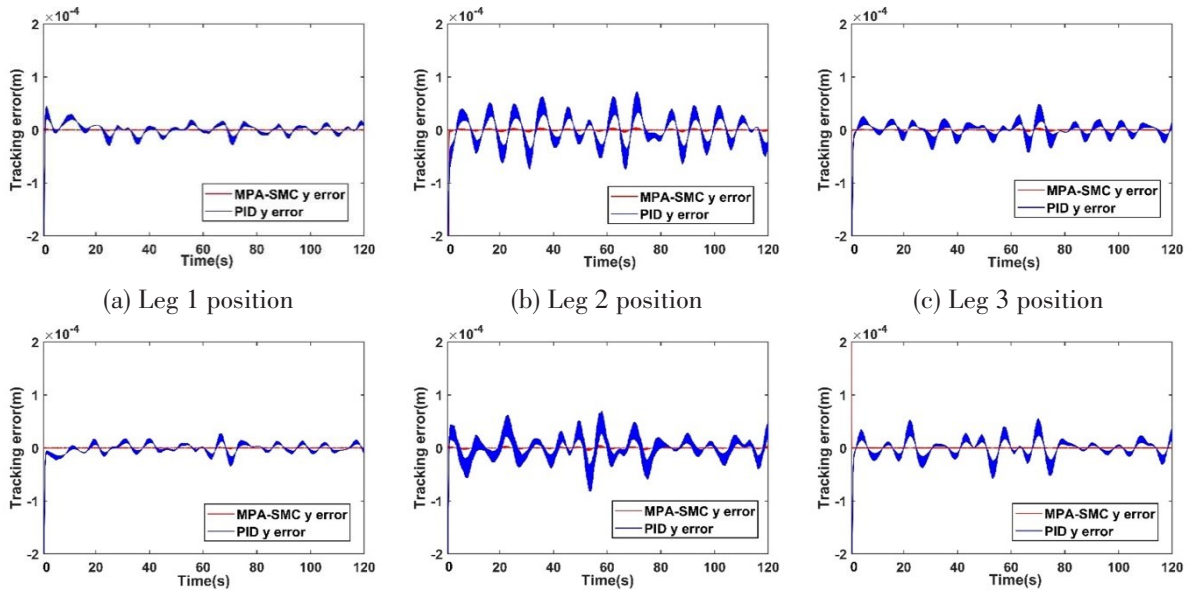


(a) Leg 1 position (b) Leg 2 position (c) Leg 3 position

(d) Leg 4 position (e) Leg 5 position (f) Leg6 position

Fig.12 Position tracking errors of two control methods

4.2.2 Anti-interference performance

To evaluate the anti-interference performance of the MPA-SMC method under disturbance imposed on the motion simulator, three types of signals, namely sinusoidal wave, square wave and random wave, are applied to controllers. The MPA-SMC is then tested and compared with the PID controller. Assuming that Leg 1 is disturbed by a sinusoidal force of 100 kN and a frequency of 0.25 rad/s, the position of Leg 1 and its position tracking error with different controllers are shown in Fig. 13. It is noteworthy that the tracking error of PID controller rises from the non-disturbance error level of $1 \times 10^{-4}$m to nearly $5 \times 10^{-4}$ m, whereas the tracking error of MPA-SMC increases only to almost $1 \times 10^{-4}$ m.

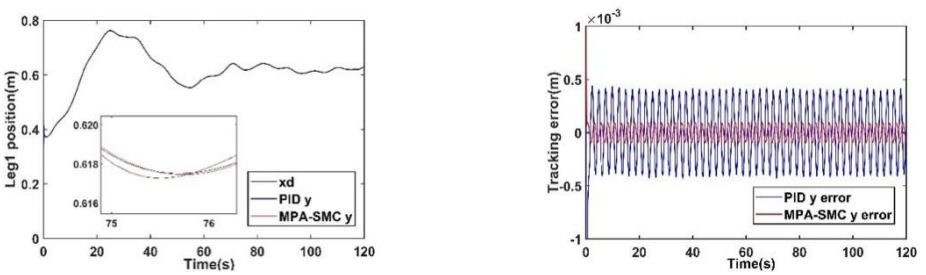


(a) Leg 1 position (b) Leg 1 position tracking error

Fig.13 Position tracking performance with a sinusoidal disturbance

Then, a sudden disturbance of 100 kN is applied to the system for evaluating the performance of controllers.As shown in Fig.14, the sudden signals occur at the tenth second, regularly appear every 20 seconds, and lasting for 4 seconds once time. It is evident that the PID controller exhibits a substantial stagger approximately $3 \times 10^{-3}$ m when the sudden load is imposed at the start of each interference, which diminishes as the interference concludes. In contrast, the MPA-SMC handles this sudden perturbation very gently and maintains its tiny error over the entire 4 seconds of each disturbance, thereby preventing the motion simulator from abruptly breaking down.

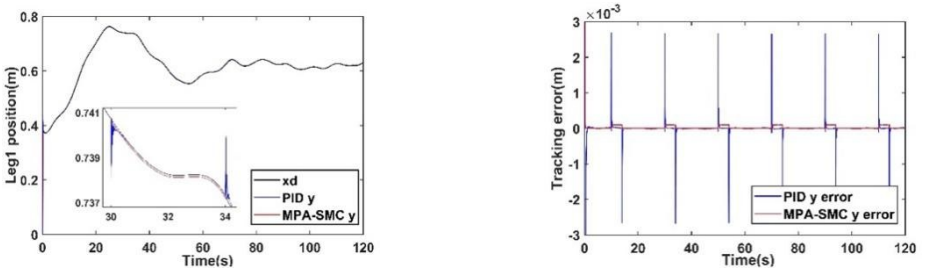


(a) Leg 1 position (b) Leg 1 position tracking error

Fig.14 Position tracking performance with a sudden disturbance

Similarly, Fig.15 demonstrates the position tracking results when random interference occurs. For the entire 120 seconds, the random disturbance force is limited to ±50 kN, the same as the amplitudes of the sinusoidal and square signals. The MPA-SMC is still superior at dealing with random interference than the well-tuned PID controller. The latter generates a tracking error of $2 \times 10^{-3}$ m, significantly large compared with the tracking error of MPA-SMC.

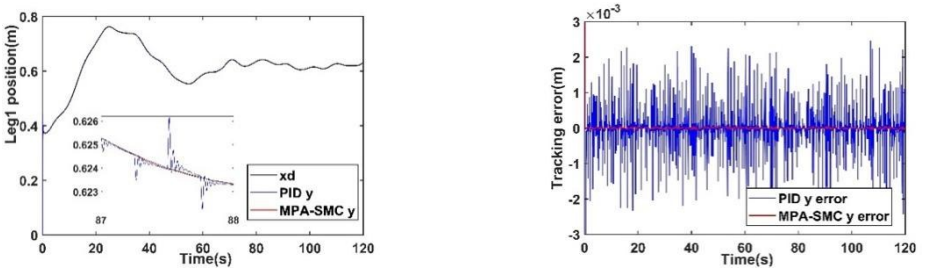


(a) Leg1 position (b) Leg1 position tracking error

Fig.15 Position tracking performance with a random disturbance

By comparing the three cases above, MPA-SMC method always outperforms PID. The former shows adequate consistency and stability no matter which kinds of disturbance it confronts, thereby achieving the objectives of column motion simulation under various interference conditions. In conclusion, the derived controller can satisfy the tracking accuracy and anti-interference requirements of the hydraulic servo system applied in the motion simulator.

## 5 Concluding remarks

Traditional motion simulators do not perform well in handling sloshing experiments with high columns. An original motion simulator for regeneration columns on floating platforms was proposed in this paper. The simulator consisted of a typical Stewart platform and a fundamental steel frame-

work to provide enough support for the platform. For safety concerns, the Stewart top platform was installed at the CoG level of the column, thus significantly reducing the offset of the CoG when column sloshing occurs. Furthermore, an MPA-SMC method was developed to control the motion simulator legs actuated by the hydraulic servo system. The MPA was integrated to optimize parameters in SMC design and improve the controller's performance. Finally, a numerical simulation was implemented using computed motions of the column under an operating sea state in MATLAB/Simulink.

The results show that both MPA-SMC and PID controller have a high accuracy within $1 \times 10^{-4}$ m without perturbations, while the former's tracking error is a slightly smaller than that of the latter. When subjected to sinusoidal, sudden, and random disturbances of 100 kN, the PID's tracking errors increase to about $5 \times 10^{-4}$ m, $3 \times 10^{-3}$ m and $2 \times 10^{-3}$ m, respectively, whereas the MPA-SMC's error level remains below $2 \times 10^{-4}$ m, demonstrating that MPA-SMC exhibits higher tracking precision and greater robustness compared to a self-tuned PID controller.

In summary, the novel motion simulator and the MPA-SMC control method enable researchers to safely conduct sloshing experiments with tall columns on floating platforms, thereby enhancing the efficiency of LNG processing units and the production capability of floating platforms. However, the proposed method is based on a virtual simulation. Some details, such as the numbers of bolts on the column skirts and the enhanced area for the top deck, need to be confirmed through real column experiments. Such information will be provided in the future. Moreover, further discussions are needed regarding peak phenomena and other potential energy consumption issues that may arise when using MPA-SMC.

## References

[1] Chretien D. Unit for establishing contact between a gas and a liquid for a floating platform: US patent 9 168, 494[P]. 2015.

[2] Son Y, Lee S, Heo S. Evaluation of the ship motion effects on the Noah/air absorption system performance[J]. Chemical Engineering Science, 2019, 207: 1049-1059.

[3] Mahmud M A, Mazumder M, Xu Q, et al. Sloshing impact on gas pretreatment for LNG plants located in a stranded offshore location[J]. Industrial & Engineering Chemistry Research, 2018, 57(17): 5764-5775.

[4] Zhang M, Li Y, Li Y, et al. Numerical simulations on the effect of sloshing on liquid flow maldistribution of randomly packed column[J]. Applied Thermal Engineering, 2017, 112: 585-594.

[5] Hanawa K, Mori M, Kouda Y, et al. An experimental study of float type LNG terminal[C]//Proceedings of the 12th International LNG Conference, International Institute of Refrigeration, 1998.

[6] Di X, Ma J, Huang Y. Mass-transfer area in a pilot-scale structured-packing column under different types of ship motion[J]. Chemical Engineering Science, 2019, 203: 302-311.

[7] Valente V T, Perondi E A. Control of an electrify diaulic Stewart platform manipulator for offshore motion compensation[C]// Proceedings of the 3rd International Conference on Mechatronics and Robotics Engineering, 2017.

[8] Zhang C, Qian Y, Dui H, et al. Component failure recognition and maintenance optimization for offshore heave compensation systems based on importance measures[J]. Journal of Loss Prevention in the Process Industries, 2020, 63: 103996.

[9] Qiao D S, Yin L, Yan J, et al. Influence of active control strategy on the motion compensation at the truncated point of mooring line[J]. China Ocean Engineering, 2021, 35(5): 700-711.

[10] Kassem A, Haddad H, Albitar C. Comparison between different methods of control of ball and plate system with 6DOF stewart platform[J]. IFAC-Papers OnLine, 2015, 48(11): 47-52.

[11] Guo H, Liu Y, Liu G, et al. Cascade control of a hydraulically driven 6-DOF parallel robot manipulator based on a sliding

mode[J]. Control Engineering Practice, 2008, 16(9): 1055-1068.
[12] Cai Y, Zheng S, Liu W, et al. Adaptive robust dual-loop control scheme of ship-mounted Stewart platforms for wave compensation[J]. Mechanism and Machine Theory, 2012, 164: 104406.
[13] Faramarzi A, Heidarinejad M, Mirjalili S, et al. Marine predators algorithm: A nature-inspired metaheuristic[J]. Expert Systems with applications, 2020, 152: 113377.
[14] Yakout A, Sabry W, Hasanien H M. Enhancing rotor angle stability of power systems using marine predator algorithm based cascaded PID control[J]. Ain Shams Engineering Journal, 2021, 12(2): 1849-1857.
[15] Chen H M, Renn J C, Su J P. Sliding mode control with varying boundary layers for an electro-hydraulic position servo system[J]. The International Journal of Advanced Manufacturing Technology, 2005, 26(1): 117-123.
[16] Won D, Kim W, Tomizuka M. High-gain-observer-based integral sliding mode control for position tracking of electrohydraulic servo systems[J]. IEEE/ASME Transactions on Mechatronics, 2017, 22(6): 2695-2704.
[17] Mingxing Y, Zhang Q, Xinliang L, et al. Adaptive sliding mode control of a nonlinear electro-hydraulic servo system for position tracking[J]. Mechanics, 2019, 25(4): 283-290.
[18] Ioannouand P A, Sun J. Robust adaptive control[M]. Courier Corporation, 2012.
[19] Han M, Du Z, Zhu H, et al. Golden-sine dynamic marine predator algorithm for addressing engineering design optimization [J]. Expert Systems with Applications, 2022, 210: 118460.

# 基于海洋捕食者算法的新型高柱晃动运动模拟器滑模控制

杜尊峰[1], 陈香玉[2], 白　浩[3], 朱海明[1], 韩沐轩[1]
(1. 天津大学 水利工程智能建设与运维全国重点实验室,天津300350; 2. 中国电建集团西北勘测设计研究院有限公司, 西安 710065; 3. 中海油能源开发装备技术有限公司南海工程分公司, 广东 湛江 524057)

**摘要:**再生塔摇晃试验对于确定海上浮式平台塔器反应性能至关重要。本研究提出一种新型塔器运动模拟装置和基于海洋捕食者算法的滑模控制器(MPA-SMC),以对安装在海上浮式平台上的高耸塔器进行摇晃试验。该运动模拟装置由Stewart平台和钢框架组成。Stewart平台位于塔器重心位置,并由钢框架提供支撑。然后,利用滑模控制方法对装置液压伺服系统进行控制,并采用海洋捕食者算法对滑模控制参数进行优化,提高控制系统的精度和鲁棒性。仿真与对比验证结果表明,新型塔器运动模拟装置在塔器摇晃试验中具有较低的扭矩,所提出的滑膜控制器在目标跟踪精度和抗干扰能力方面比传统PID控制器表现更好。

**关键词:** 反应塔; 晃动实验; 运动模拟器; Stewart平台; 滑模控制; 海洋捕食者算法
**中图分类号:** TE952　　**文献标识码:** A
**基金项目:** 国家重点研发计划项目(2022YFC2806300);国家自然科学基金资助项目(51109158);
天津市交通科技发展项目(2022-48);天津大学研究生教育专项基金资助项目(C1-2021-004);
天津市研究生科研创新项目(2022BKY077)

**作者简介:** 杜尊峰(1984-),男,博士,天津大学副教授;
陈香玉(1997-),女,硕士,中国电建集团助理工程师;
白　浩(1986-),男,中海油能源开发装备技术有限公司高级工程师;
朱海明(1992-),男,博士,天津大学助理研究员;
韩沐轩(1996-),女,博士研究生。